Journal of Alloys and Compounds 503 (2010) L34–L39

Contents lists available at ScienceDirect

Journal of Alloys and Compounds

journal homepage: www.elsevier.com/locate/jallcom

Letter

Catalyst-free synthesis, morphology evolution and optical property of one-dimensional aluminum nitride nanostructure arrays

Haibing Li[a], W.J. Wang[b], B. Song[c], R. Wu[a], J. Li[a], Y.F. Sun[a], Y.F. Zheng[a], J.K. Jian[a,*]

[a] Department of Physics, Xinjiang University, No. 14, Shengli Road, Urumqi 830046, Xinjiang, PR China
[b] Institute of Physics, Chinese Academy of Sciences, Beijing 100190, PR China
[c] Academy of Fundamental and Interdisciplinary Sciences, Harbin Institute of Technology, Harbin 150080, PR China

ARTICLE INFO

Article history:
Received 25 January 2010
Received in revised form 4 May 2010
Accepted 4 May 2010
Available online 12 May 2010

Keywords:
Nanostructured materials
Aluminum nitride
Vapor deposition
Morphology
Microstructure

ABSTRACT

One-dimensional (1D) aluminum nitride (AlN) nanorod and nanocolumn arrays have been synthesized on graphite sheets, silicon and molybdenum (Mo) plates through a catalyst-free chemical vapor deposition (CVD) process employing $AlCl_3$ and NH_3 as sources. The as-prepared nanorods and nanocolumns vertically grow on the substrates with high alignment along [0 0 1] orientation of hexagonal AlN. Different AlN nanostructures, including hollow nanospheres, nanorod and nanocolumn arrays, roll-like hierarchical structures and nanoparticles, can be readily synthesized by adjusting the growth parameters. The morphological evolution of those nanostructures is addressed based on the vapor solid (VS) growth combined with the surface diffusion process. The photoluminescence and Raman scattering properties of the AlN nanorod and nanocolumn arrays are examined.

1. Introduction

Low dimensional nanostructures have attracted great interest from both fields of science and technology due to their unique properties and potential technological applications [1–3]. As an important wide-gap semiconductor, aluminum nitride can be applied in a variety of optoelectronic devices and field emission (FE) devices because of its special physical properties, such as high thermal conductivity, high piezoelectric response, low dielectric loss, excellent mechanical strength and chemical stability [4–6]. Recently, researchers have reported some AlN nanostructures including nanowires [7–9], nanotubes [10,11], nanospheres [12,13], nanobelts [14], nanocones [15], nanotips [16], nanorods [17–19] and hierarchical nanostructures [20–22]. More recently, several novel approaches have been developed to synthesize AlN nanostructures and some interesting results have been reported. Sun et al. synthesized hollow AlN fibers through carbothermal reduction and nitridation of electrospun precursor fibers [23]. Shi et al. reported a combustion route to obtain quasi-aligned AlN nanowhiskers at a low nitrogen gas pressure [24,25]. Using the high temperature direction nitridation method, Lei et al. synthesized straight and stacked-sheet AlN nanowires with high purity [26]. Through the direction reaction between $AlCl_3$ and NaN_3, hexagonal AlN microbelts were grown at a temperature of 450 °C in autoclaves under a dry and pure nitrogen environment [27]. By introducing CaF_2 as dispersant, Yu et al. developed a low-temperature CVD method to grow AlN nanorods [28]. Arc discharge method has also been used to synthesize ripple-like AlN nanowires and urchin-like AlN nanostructures [29,30]. Moreover, some aligned one-dimensional (1D) nanostructures of AlN have been synthesized, which is of great importance for their applications. Liu et al. [15] reported that AlN quasi-aligned nanocone arrays were synthesized on silicon or quartz wafers by a catalyst-assisted vapor solid growth via the reaction between $AlCl_3$ vapors and NH_3 gas. They pointed out that the catalysts, such as Ni, Fe and Co, played key roles for the growth of those AlN nanocones [15]. Another group synthesized aligned nanotips, brushes and complex nanostructures of AlN on silicon substrates by CVD technique, and found the morphologies of the products could be affected by the orientation of silicon substrates [31].

Despite some success on the growth of AlN nanostructures, it is still highly valuable to achieve the controlled growth of well-aligned AlN 1D nanostructure arrays on different substrates. Herein, for the first time, we reported a catalyst-free and morphology-controlled growth of AlN nanorod and nanocolumn arrays on different substrates, including conducting and flexible graphite sheets, metallic Mo plates and silicon. The AlN nanorod arrays grown on conducting graphite sheets and Mo plates could be a good candidate for field emission applications. In particular, the flexibility of graphite sheets is beneficial to the potential appli-

* Corresponding author. Tel.: +86 991 8583183; fax: +86 991 8582405.
E-mail address: jikangjian@gmail.com (J.K. Jian).

0925-8388/$ – see front matter © 2010 Elsevier B.V. All rights reserved.
doi:10.1016/j.jallcom.2010.05.021

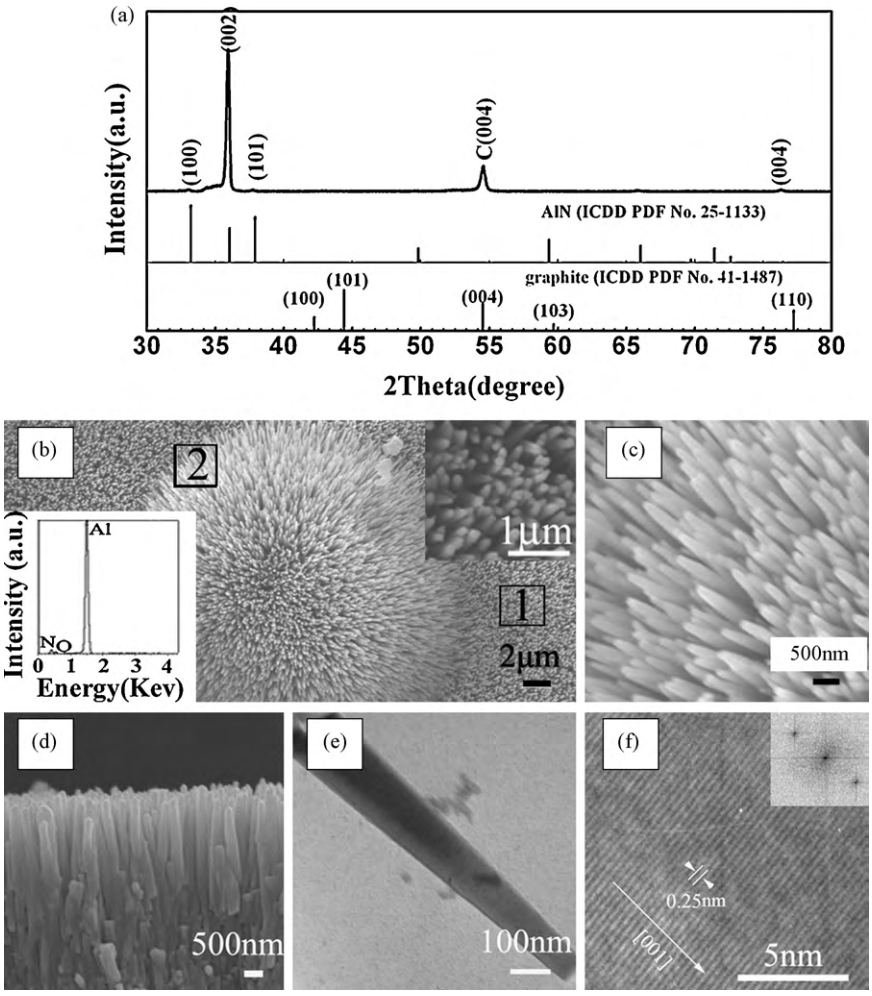

Fig. 1. (a) XRD pattern of the product grown on graphite sheets at 25–30 cm away from the center of tube under the heating temperature of 800 °C. The standard XRD data of hexagonal AlN and graphite are shown at the bottom. (b) Top-view low-magnification SEM image and EDX (the bottom-left inset) of the product. The up-right inset is the enlargement of the boxed region 1. (c) High-magnification SEM image of the boxed region 2 in (b). (d) The cross-section view SEM image of the AlN nanorod array. (e) TEM image of an individual AlN nanorod. (f) HRTEM image of an AlN nanorod showing its growth along [0 0 1] direction. The inset is the corresponding fast Fourier transform image.

cations of the AlN nanorod arrays in flexible field emission displays. The morphologies of the AlN nanostructures synthesized here can be turned from hollow nanoparticles to nanorod arrays by adjusting the synthetic parameters. The photoluminescence and Raman scattering properties of the nanostructure arrays were studied. The results demonstrated the feasibility of controlled growth of AlN 1D nanostructure arrays with desired morphology by a catalyst-free CVD process, which should be helpful to facilitate their applications.

2. Experimental

The syntheses of AlN nanostructures were carried out in a typical chemical vapor deposition system which consists of a horizontal tubular electric resistance furnace with a pumping system and a gas supply system. Anhydrous $AlCl_3$ (97.91%) and NH_3 gas were served as aluminum and nitrogen sources. Graphite sheets, silicon (1 0 0) and Mo plates were used as substrates for the deposition of the products. No catalyst was intentionally used. In a typical run, appropriate amount of $AlCl_3$ powder was placed at the upstream side of the furnace and the substrates were put on the zone separated from Al source about 10–40 cm. When the system was evacuated to a vacuum of about 7×10^{-3} Pa, an Ar flow of 100 standard cubic centimeters per minute (sccm) was introduced into the system. Then the temperature of the furnace was raised to a desired temperature and a NH_3 flow of 200 sccm was started and maintained for 4 h. After that, the NH_3 flow was shut down and the system was cooled to ambient temperature under the same Ar flow. The products deposited on the substrates were characterized by X-ray diffraction (XRD, Mac Science M18XHF22-SRA), scanning electron microscopy (SEM, LEO 1430VP) equipped with an energy-dispersive X-ray (EDX) analyzer attachment, transmission electron microscopy (TEM, Hitachi H-600) and high-resolution transmission electron microscopy (HRTEM, JEOL JEM-2100). Photoluminescence (PL) spectra of the products were taken at the room temperature using the 325 nm of He–Cd laser with a Hitachi F-4500 spectrofluorometer. Raman measurements were performed on a JY-HR800 laser Raman spectrometer using a 532 nm solid-state laser as excitation source.

3. Results and discussion

Fig. 1(a) shows the XRD pattern of the product deposited on graphite sheet at the upstream zone (denoted as zone 1) of the tube with a distance of 25–30 cm away from the center of the tube, where the temperature is about 560–420 °C. The standard diffraction data of wurtzite-structured AlN (ICDD PDF No. 25-1133) and graphite (ICDD PDF No. 41-1487) are also shown at the bottom of Fig. 1(a). Two main reflections locating at about 35.9° and 54.5° are clearly observed, which can be assigned to (0 0 2) reflection of wurtzite-structured AlN and (0 0 4) reflection of graphite, respectively. Except three very weak reflections of AlN ((1 0 0), (1 0 1), (0 0 4) at 33.1°, 37.8° and 76.2°, respectively), no other peak is observed in the pattern, indicating that the AlN product has a strong preferred orientation along [0 0 1]. Fig. 1(b) is a low-magnification SEM image, giving an overall view of the product. It can be seen that the product consists of a large amount of AlN nanorods which are uniform and vertically aligned to form regular array. The bottom-left inset of Fig. 1(b) is an EDX spectrum taken from the product,

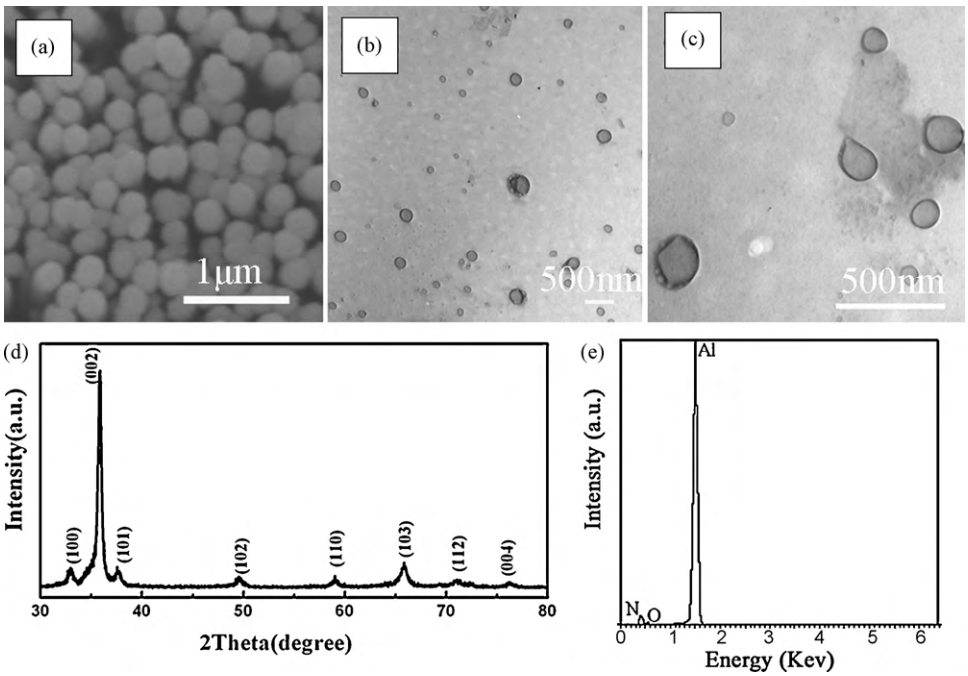

Fig. 2. (a) SEM, (b) low-magnification TEM image and (c) high-magnification TEM image of the AlN hollow nanospheres grown on graphite sheets under the heating temperature of 800 °C. (d) XRD pattern and (e) EDX of the AlN hollow nanospheres.

indicating that the product is mainly composed of Al and N with a molar ratio of about 1:1. A trace amount impurity of O was detected, which probably comes from residual oxygen in the system. The up-right inset of Fig. 1(b) is an enlarged top-view SEM image of the boxed region 1, revealing the high density of the nanorod array. Interestingly, some hemisphere-like structures assembled by radially-aligned nanorods can be found in the product. Fig. 1(c) is a high-magnification SEM image of the boxed region 2 in Fig. 1(b), which displays that the AlN nanorods have cone-like outer shape, i.e. so-called nanocone [15] with sharp tip and thick bottom. A cross-section SEM image in Fig. 1(d) shows the high density and regular arrangement of the AlN nanorod array. The TEM morphological image (Fig. 1(e)) of an individual AlN nanorod displays its smooth surface and tapered outer shape. The HRTEM image of a AlN nanorod (Fig. 1(f)) presents clear lattice fringes with a spacing of 0.25 nm, which is in agreement with the spacing of (0 0 2) planes of wurtzite AlN (ICDD PDF No. 25-1133). The inset is the corresponding fast Fourier transform (FFT) of the HRTEM. The TEM examinations indicate that the AlN nanorod is single crystal and grows along [0 0 1] direction. The results of SEM and TEM studies are consistent with that of XRD analysis. It is worth noting that the cone-like AlN nanorod array is first time synthesized on conducting and flexible graphite sheet by a catalyst-free CVD process although similar structure has been reported before [15].

Under the same heating temperature of 800 °C, the morphologies of the products deposited on different positions of the tube are different. At the center of the tube (heating zone, denoted as zone 2), many AlN hollow spheres are obtained on the graphite sheets. Fig. 2(a), and (b) as well as (c) is SEM and TEM images of the AlN hollow spheres, respectively. The SEM image displays the sphere-like morphology of the product. The TEM images show lighter contrast in the core area while darker in the shell of those spheres, which reveals that the spheres are hollow inside. The diameters of hollow spheres range about from 100 nm to 300 nm. Fig. 2(d) is the XRD pattern of those AlN hollow spheres, revealing their wurtzite structure. Compared with the XRD pattern of AlN nanorod array, more reflections are detected, indicating a weaker preferred orientation of the products. EDX analysis (Fig. 2(e)) reveals that there is also a small amount of O impurity in the products. Zhang et al. [12] synthesized AlN hollow nanospheres by post-annealing the intermediate template $AlCl_3{\cdot}xNH_3$@AlN core–shell nanostructures. Here, no such intermediate product has been observed and the hollow AlN spheres were obtained by a one-step growth.

To further examine the effect of the heating temperature on the morphologies of the products, a series of controlled syntheses were performed under the heating temperature from 800 °C to 1100 °C while maintaining graphite sheets as substrates. SEM images shown in Fig. 3(a) illustrate the morphological evolution of the AlN products (nanospheres, nanorods, nanocolumns, micro-particles and nanoparticles) grown for 4 h under the different heating temperature. It can be seen that the products deposited on the zone 1 remain nanorod-like morphology when the heating temperature increases from 800 °C to 1000 °C. Careful SEM observation reveals the slope of the nanorods' diameter along their axis decreases, i.e. the more uniform diameter along their growth direction. While the heating temperature increases to 1100 °C, the morphology of the product deposited at the zone 1 becomes micro-sized particles. For the products grown at the zone 2, their morphologies change from nanospheres to 1D nanostructures when the heating temperature increases from 800 °C to 1000 °C. Those 1D nanostructures have flat top and regular hexagonal prism-like outer shape, and hence are called nanocolumns [15]. The morphological features are quite different from those of cone-like nanorods grown on the zone 1 where the temperature is lower than that of the zone 2. The nanocolumns vertically grow on the substrates forming arrays, too. When the heating temperature increases to 1100 °C, the product is composed of a large number of nanoparticles. Fig. 3(b) presents a temperature profile of the furnace when the heating temperature is 1000 °C, revealing the temperature distribution of the system.

The growth of the AlN nanorods and nanocolumns was unlikely to follow the well-known vapor–liquid–solid (VLS) mechanism [32] because that no evidence for the existence of liquid-phase species was found. It is reasonable to think that their growth should be dominated by a vapor solid (VS) process and similar with those reported in the literature [15]. Briefly, gaseous AlN species were firstly formed by the reaction between the vaporized $AlCl_3$ and NH_3.

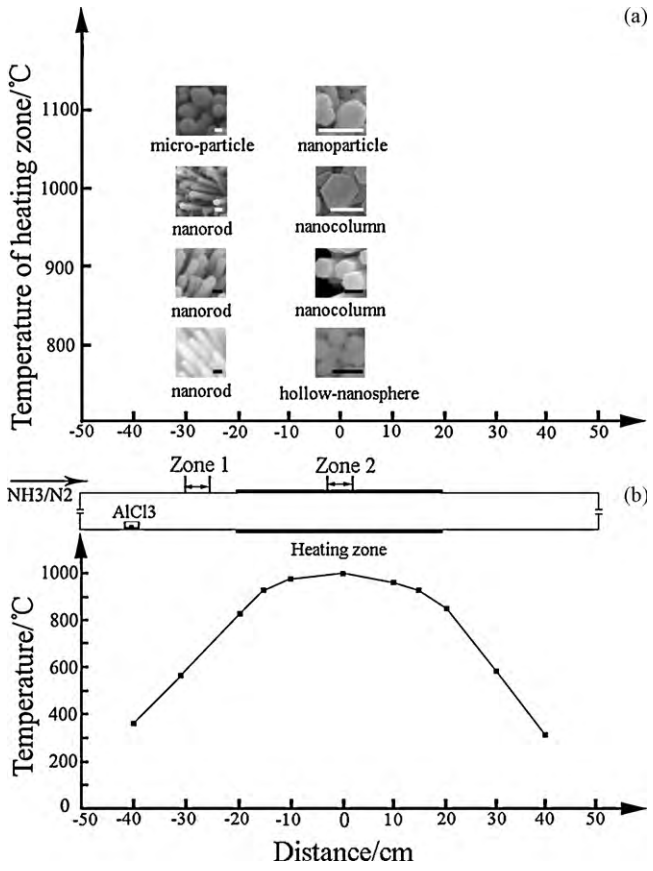

Fig. 3. (a) The morphological dependence of AlN nanostructures on the heating temperature and the deposition position on graphite sheet substrate. All scale bars are 300 nm. (b) Corresponding temperature profile of the furnace when the heating temperature is 1000 °C.

When the incidence gaseous species reached the suitable supersaturation in the system, they would precipitate, nucleate and grow into finally solid products. Among those processes, the supersaturation plays a key role for the 1D growth of the products. It is generally accepted that a proper supersaturation is a critical factor for 1D nanostructures grown from vapor phase. Under a proper supersaturation, the incidence AlN species should be preferred adsorbed and incorporated into (0 0 1) plane of AlN crystal due to its asymmetry crystal structure along this direction [10], which results in the formation of finally 1D nanostructures. As to the cone- or column-like morphology of the 1D nanostructures, the surface-migration of the AlN species should be responsible for it [15]. Higher temperature would result in a higher surface-migration rate of the AlN species, which is favorable for the formation of nanocolumns with uniform diameters along their axis. Our observation that the higher temperature would lead to the growth of AlN nanocolumns is consistent with the previous report [15,33], and supports the above deduction, too. As seen from Fig. 3(a), the morphologies of the products deposited on the different positions are different. In our system, the AlN species supersaturation at the zone 1 should be higher than that of the zone 2 because it is nearer to $AlCl_3$ source with lower temperature. When the heating temperature is 800 °C, the supersaturation of the zone 2 is too low to sustain the 1D growth, so no 1D nanostructure was formed. When the heating temperature is 1100 °C, the supersaturations of both zones become very large due to the great enhanced vaporization of $AlCl_3$ source and reaction with NH_3. Such a large supersaturation cannot support the oriented growth of 1D nanostructures and just results in the formation of particle-like products. When the heating temperatures are 900 °C and 1000 °C, the products at the zone 2 are nanocolumns instead of cone-like nanorods, which can be addressed by the aforementioned surface-migration process.

Notably, we found that AlN hexagonal prism-like nanocolumn arrays could be grown on different substrates. As mentioned above, the AlN nanocolumn arrays were successfully synthesized on graphite sheets at the zone 2 with the heating temperature of 900 °C. Fig. 4(a) clearly displays its morphological feature. When substituting the substrates of Si (1 0 0) or Mo plates for graphite sheet and fixing other conditions, as seen from Fig. 4(b) and (c), AlN nanocolumn arrays were synthesized, too. It can be seen that the AlN nanocolumn arrays grown on Si (1 0 0) substrate have a high density and almost form a continuous film. Compared with those cone-like nanorods, all the nanocolumns grown on graphite and Si are well faceted, suggesting their higher crystallinity. The XRD pattern (Fig. 4(g)) of the AlN nanocolumn arrays on Si (1 0 0) substrate presents much stronger [0 0 1] preference and sharper profiles of peaks compared with that of the nanocolumn arrays on Mo plate (Fig. 4(h)). Such difference should be due to the higher alignment and density, as well as larger diameters of the nanocolumns grown on Si substrate, as revealed by SEM observations. The strongest peak in the pattern is due to (4 0 0) reflection of Si substrate. The products grown on Mo plate at zone 1 under 900 °C are the mixture of nanoparticles and small nanorods, while only particles are formed on Mo plate at zone 2 under 1000 °C. Interestingly, when the heating temperature was 1000 °C, as shown in Fig. 4(d), some free-standing AlN roll-like hierarchical structures with micron sizes were formed on Mo plate at the zone 1. Fig. 4(e) and (f) shows the local-magnification SEM images of these AlN micro-roll-like structures, revealing the details of their structures. It can be seen that the roll-like structures are assembled by the high density nanorods with much smaller diameters than those of nanocolumns. The XRD pattern (Fig. 4(i)) of the sample shows very strong reflections of Mo substrate (ICDD PDF No. 42-1120). The peaks of wurtzite AlN become weak and broad. The preference of AlN [0 0 1] reflection decreases than that of nanorod or nanocolumns arrays. Some unknown peaks marked by "*" are also detected. From SEM images of the sample, one can find that those roll-like structures randomly distribute on Mo plate and do not totally cover the substrate, which should be the reason for such a XRD pattern. Such interesting AlN self-assembly nanostructures have not been reported before. It can be speculated that two possible reasons should be responsible for their formation. The first one is the large lattice mismatch between the AlN (0 0 1) and Mo plate. It is known that the crystal structure of hexagonal graphite is similar with that of AlN while Mo has a body-centered cubic structure. In addition, the graphite sheets used here are [0 0 1] oriented and Mo plates are polycrystalline. So there are larger structural mismatch between the Mo plates and AlN layer than that between graphite and AlN layer. Consequently, there is larger stress in the grown AlN layer. Chen et al. also reported brush-like complex AlN nanostructures grown on Si (1 0 0) and thought its formation was due to the large lattice mismatch [31]. The second important factor should be the growth rate. As shown in Fig. 4, there is no roll-like AlN complex nanostructure grown on Mo plate in the zone 2 under a temperature of 900 °C, while the roll-like AlN complex nanostructures were grown in the zone nearer the source and the heating temperature is raised to 1000 °C. It can be expected that there is a higher growth rate of the AlN products under higher temperature and concentration of source, which results in the fast accumulation of stress in the interface layer between AlN and Mo substrate due to their large structural mismatch. To release the stress, the grown AlN nanostructures have a tendency to roll up forming roll-like structures.

The PL spectra of the AlN nanorod and nanocolumn arrays are shown in Fig. 5. It can be seen that both spectra present similar broad blue emission bands centered at 2.57 eV (nanocolumns),

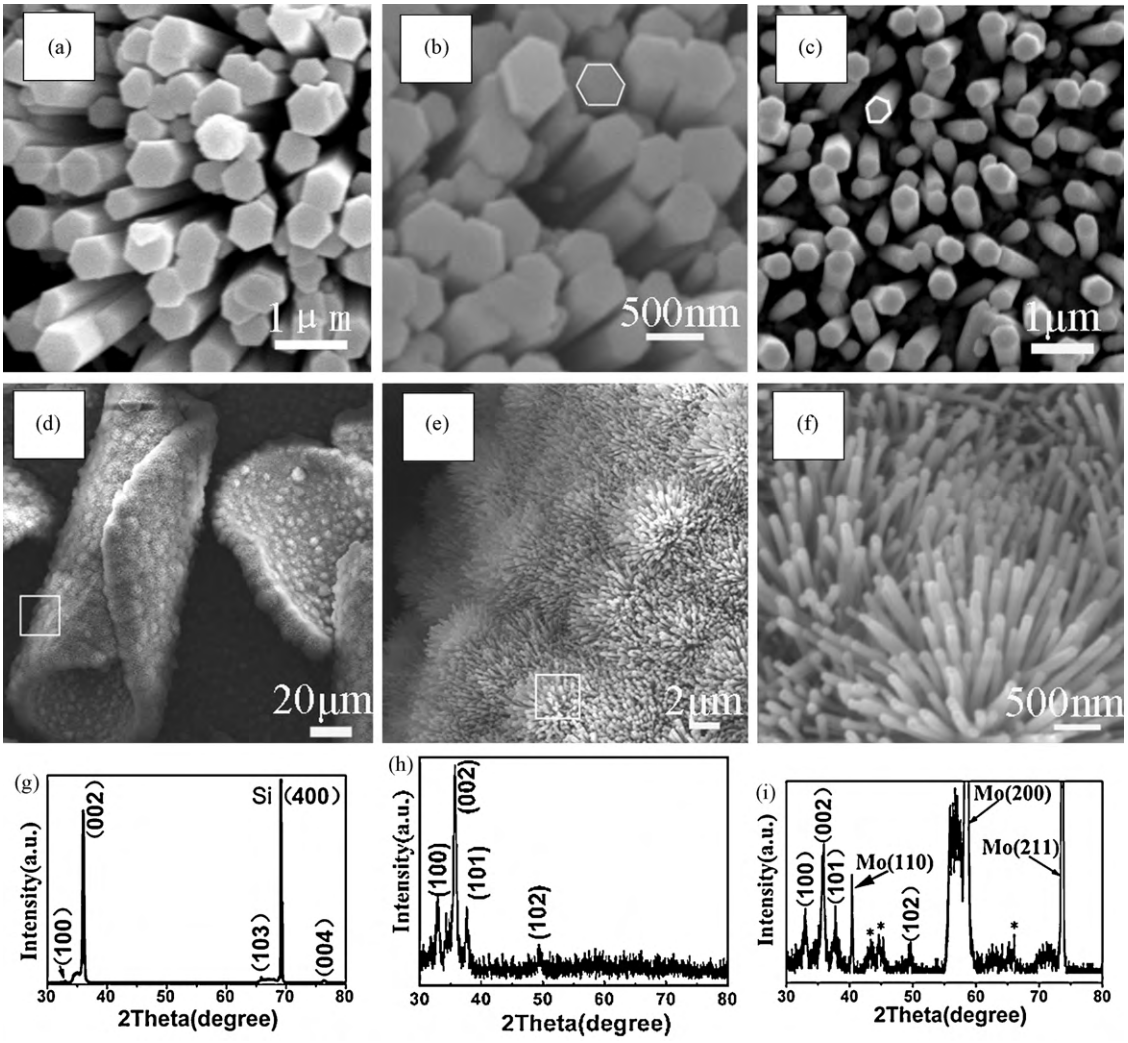

Fig. 4. SEM images of AlN nanocolumn arrays grown on (a) Graphite sheets, (b) Si (1 0 0) substrate and (c) Mo plate at the heating zone with the heating temperature of 900 °C. (d) Low-magnification SEM image of the AlN roll-like structures grown on Mo plate at the upstream side with a distance of 25 cm away from the center of tube, and the heating temperature is 1000 °C. (e) The enlargement of the boxed region of (d). (f) High-magnification SEM images of the boxed area shown in (e). (g)–(i) are XRD patterns of nanocolumn arrays on Si, Mo and roll-like structures on Mo, respectively. Some unknown peaks in (i) are marked by "*".

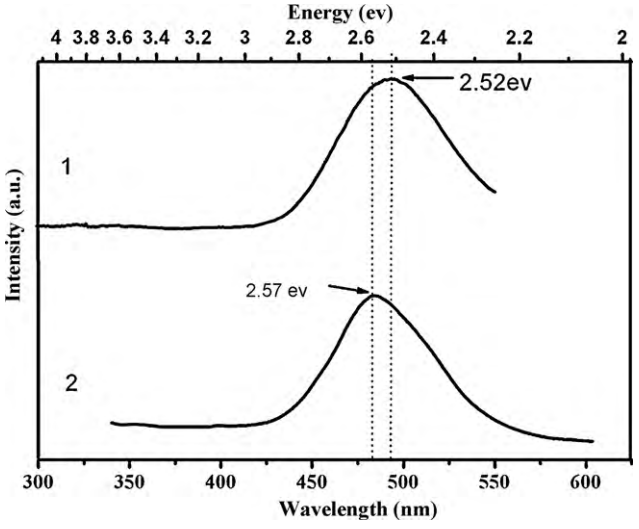

Fig. 5. PL spectra of AlN nanorod arrays (1) and nanocolumn arrays (2) grown on graphite sheets under the heating temperature of 800 °C and 900 °C, respectively.

and 2.52 eV (nanorods), respectively. The PL emission of the nanocolumns has a small blue shift compared with that of nanorods. The higher crystalline quality of the nanocolumns is possible reason for it. This band is not due to the direct bad gap emission of AlN because of its large band gap with a value of about 6.2 eV [15]. So it should be assigned to a defect- or impurity-related level emission. Such emission band has been observed in some AlN nanostructures with different morphologies, including nanocones [15], urchin-like and flower-like nanostructures [22]. Ref. [34] attributed the emission to the nitrogen vacancy and the radioactive recombination of a photo-generated hole with an electron occupying the nitrogen vacancy. The oxygen impurity [22,34] is thought to be another possible reason for the band because a trace amount of oxygen impurity was always detected in our samples.

Raman scattering was further employed to examine the phonon modes of the AlN nanorod and nanocolumn arrays. The patterns 1 and 2 shown in Fig. 6 are their corresponding Raman spectra, respectively. According to the group theory, there are six first-order Raman-active modes of hexagonal AlN, i.e. $1A_1(TO) + 1A_1(LO) + 1E_1(LO) + 1E_1(TO) + 2E_2$, because it belongs to the space group $P6_3mc$ with all atoms occupying the C_{3v} sites [35]. From Fig. 6, it can be seen that only one obvious band at 655 cm^{-1}

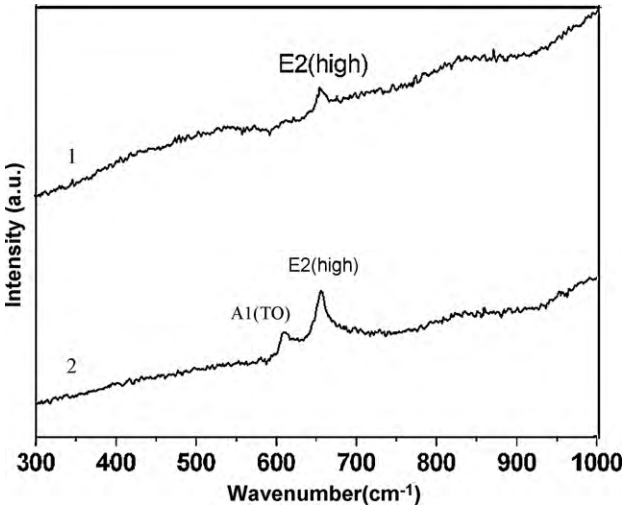

Fig. 6. Raman spectra of AlN nanorod arrays (1) and nanocolumn arrays (2) grown on graphite sheets under the heating temperature of 800 °C and 900 °C, respectively.

presents in the pattern 1 and two bands at 610 cm^{-1} and 656 cm^{-1} present in the pattern 2. Based on the previous reports [10,14], the low and high frequency bands can be assigned to A_1 (TO) and E_2 (high) phonon modes of h-AlN, respectively. These Raman peaks have asymmetric and broadened profiles, which can be explained by the small-size effects and the internal stress of the nanorod and nanocolumn arrays [10]. In addition, E_2 (high) peak of the nanocolumns is sharper and stronger than that of the nanorods, which implies better crystallinity of the nanocolumns, too. Such result is reasonable because the nanocolumns are grown at a higher temperature, and it is consistent with the results of SEM observations, too. Another feature of the two spectra is the absences of several phonons (such as A_1(LO), E_1(LO) and E_1(TO)), which is believed to be due to the special angle between of the incident phonons and the aligned AlN nanorod and nanocolumn arrays in the near backscattering geometry [15,14,36]. A_1(TO) phonon mode is not present in the spectrum of nanorod arrays compared with that of nanocolumn arrays. It is possible due to the small difference between the two morphologies which result in the different angles between the incident light and two kinds of nanostructure arrays.

4. Conclusions

In summary, AlN nanostructures, including hollow nanospheres, aligned nanorod and nanocolumn arrays and roll-like hierarchical structures, have been synthesized by a chemical vapor deposition procedure without the assistant of any catalyst. The XRD, SEM and TEM characterizations indicate that those nanorod and nanocolumn arrays are perpendicular to substrates and grow along [0 0 1] direction of *h*-AlN. The morphologies of those AlN nanostructures can be tuned by adjusting the heating temperature, growth position and the choices of the substrates. A VS growth mechanism combined with surface diffusion process has been applied to address their morphological evolution. The Raman band profiles of the AlN nanorod and nanocolumn arrays presents size- and stress-related broadening and asymmetry. Their PL spectra present a broad blue emission at 483 nm, suggesting they may have applications in optoelectronic nanodevices.

Acknowledgments

This work is supported by the National Natural Science Foundation of China (grant nos. 50862008, 50702073, 10864004), and the National Basic Research Program of China (973 Program) with grant no. 2007CB936300.

References

[1] Y. Cui, Q.Q. Wei, H. Park, C.M. Lieber, Science 293 (2001) 1289.
[2] Y. Zhang, T. Ichihashi, E. Landree, F. Nihey, S. Lijima, Science 285 (1999) 1719.
[3] Z.W. Pan, Z.R. Dai, Z.L. Wang, Science 291 (2001) 1947.
[4] Y. Taniyasu, M. Kasu, T. Makimoto, Appl. Phys. Lett. 84 (2004) 2115.
[5] Q. Zhao, J. Xu, X.Y. Xu, Z. Wang, P.D. Yu, Appl. Phys. Lett. 85 (2004) 5331.
[6] Y.B. Tang, H.T. Cong, H.M. Cheng, Appl. Phys. Lett. 89 (2006) 093113.
[7] Y.J. Zhang, J. Liu, R.R. He, Q. Zhang, X.Z. Zhang, J. Zhu, Chem. Mater. 13 (2001) 3899.
[8] Q. Wu, Z. Hu, X.Z. Wang, Y.N. Lu, K.F. Hu, S.Z. Deng, N.S. Xu, B. Shen, R. Zhang, Y. Chen, J. Mater. Chem. 13 (2003) 2024.
[9] H.M. Lv, G.D. Chen, H.G. Ye, G.J. Yan, J. Appl. Phys. 101 (2007) 053526.
[10] Q. Wu, Z. Hu, X.Z. Wang, Y.N. Lu, X. Chen, H. Xu, Y. Chen, J. Am. Chem. Soc. 125 (2003) 10176.
[11] L.W. Yin, Y. Bando, Y.C. Zhu, M.S. Li, C.C. Tang, D. Golbery, Adv. Mater. 17 (2005) 213.
[12] F. Zhang, Z. Hu, Q. Wu, P. Xiao, Y.W. Ma, Y.M. Hu, X.Z. Wang, C.Y. Wang, J. Phys. Chem. C 112 (2008) 11331.
[13] J. Zheng, X.B. Song, Y.H. Zhang, Y. Li, X.G. Li, Y.K. Pu, J. Solid State Chem. 180 (2007) 276.
[14] Q. Wu, Z. Hu, X.Z. Wang, Y. Chen, Y.N. Lu, J. Phys. Chem. B 107 (2003) 9726.
[15] C. Liu, Z. Hu, Q. Wu, X.Z. Wang, Y. Chen, H. Sang, J.M. Zhu, S.Z. Deng, N.S. Xu, J. Am. Chem. Soc. 127 (2005) 1318.
[16] S.C. Shi, C.F. Chen, S. Chattopadhyay, Z.H. Lan, K.H. Chen, L.C. Chen, Adv. Funct. Mater. 15 (2005) 781.
[17] J.H. He, R. Yang, Y.L. Chueh, L.J. Chou, L.J. Chen, Z.L. Wang, Adv. Mater. 18 (2006) 650.
[18] Y.B. Tang, H.T. Cong, Z.G. Zhao, H.M. Cheng, Appl. Phys. Lett. 86 (2005) 153104.
[19] X.B. Song, Z.G. Guo, J. Zheng, X.G. Li, Y.K. Pu, Nanotechnology 19 (2008) 115609.
[20] L.W. Yin, Y. Bando, Y.C. Zhu, M.S. Li, Y.B. Li, D. Golberg, Adv. Mater. 17 (2005) 110.
[21] Q. Wu, F. Zhang, X.Z. Wang, C. Liu, Z. Hu, Y.N. Lu, J. Phys. Chem. C 111 (2007) 12639.
[22] F. Zhang, Q. Wu, X.B. Wang, N. Liu, J. Yang, Y.M. Hu, L.S. Yu, X.Z. Wang, Z. Hu, J.M. Zhu, J. Phys. Chem. C 113 (2009) 4053.
[23] Y. Sun, J.Y. Li, Y. Tan, L. Zhang, J. Alloys Compd. 471 (2009) 400.
[24] Z.Q. Shi, M. Radwan, S. Kirihara, Y. Miyamoto, Z.H. Jin, J. Alloys Compd. 476 (2009) 360.
[25] Z.Q. Shi, M. Radwan, S. Kirihara, Y. Miyamoto, Z.H. Jin, Ceram. Int. 35 (2009) 2727.
[26] M. Lei, H. Yang, P.G. Li, W.H. Tang, J. Alloys Compd. 459 (2008) 338.
[27] H.L. Wang, H.M. Lv, G.D. Chen, H.G. Ye, J. Alloys Compd. 477 (2009) 580.
[28] L.S. Yu, N. Liu, X.B. Wang, Z. Hu, J. Alloys Compd. 478 (2009) 121.
[29] W.W. Lei, D. Liu, J. Zhang, Q.L. Cui, G.T. Zou, Cryst. Growth Des. 9 (2009) 1489.
[30] L.H. Shen, X.F. Li, Q.L. Cui, B.B. Liu, T. Cui, Appl. Phys. A 99 (2010) 111.
[31] Z. Chen, C.B. Cao, H.S. Zhu, J. Phys. Chem. C 111 (2007) 1895.
[32] R.S. Wagner, W.C. Ellis, Appl. Phy. Lett. 4 (1964) 89.
[33] J. Zheng, Y. Yang, B. Yu, X.B. Song, X.G. Li, ACS Nano 2 (2008) 134.
[34] Y.G. Cao, X.L. Chen, Y.C. Lan, J.Y. Li, T. Xu, Y.P. Xu, Q.L. Liu, J.K. Liang, J. Cryst. Growth 213 (2002) 198.
[35] M.S. Liu, L.A. Bursill, S. Prawer, K.W. Nugent, Y.Z. Tong, G.Y. Zhang, Appl. Phy. Lett. 74 (1999) 3125.
[36] S.C. Lyu, O.H. Cha, E.K. Suh, H. Ruh, H.J. Lee, C.J. Lee, Chem. Phys. Lett. 367 (2003) 136.